Bnip3 mediates doxorubicin-induced cardiac myocyte necrosis and mortality through changes in mitochondrial signaling

Rimpy Dhingra[a], Victoria Margulets[a], Subir Roy Chowdhury[a], James Thliveris[b], Davinder Jassal[a,c], Paul Fernyhough[a,d], Gerald W. Dorn II[e], and Lorrie A. Kirshenbaum[a,d,1]

[a]Department of Physiology and Pathophysiology, [b]Department of Anatomy and Cell Science, [c]Department of Medicine, Faculty of Health Sciences, and [d]Department of Pharmacology and Therapeutics, Institute of Cardiovascular Sciences, St. Boniface Hospital Research Centre, University of Manitoba, Winnipeg, MB, Canada R2H 2H6; and [e]Center of Pharmacogenetics, Department of Internal Medicine, Washington University School of Medicine, St. Louis, MO 63110

Edited* by Eric N. Olson, University of Texas Southwestern Medical Center, Dallas, TX, and approved November 3, 2014 (received for review August 4, 2014)

Doxorubicin (DOX) is widely used for treating human cancers, but can induce heart failure through an undefined mechanism. Herein we describe a previously unidentified signaling pathway that couples DOX-induced mitochondrial respiratory chain defects and necrotic cell death to the BH3-only protein Bcl-2-like 19kDa-interacting protein 3 (Bnip3). Cellular defects, including vacuolization and disrupted mitochondria, were observed in DOX-treated mice hearts. This coincided with mitochondrial localization of Bnip3, increased reactive oxygen species production, loss of mitochondrial membrane potential, mitochondrial permeability transition pore opening, and necrosis. Interestingly, a 3.1-fold decrease in maximal mitochondrial respiration was observed in cardiac mitochondria of mice treated with DOX. In vehicle-treated control cells undergoing normal respiration, the respiratory chain complex IV subunit 1 (COX1) was tightly bound to uncoupling protein 3 (UCP3), but this complex was disrupted in cells treated with DOX. Mitochondrial dysfunction induced by DOX was accompanied by contractile failure and necrotic cell death. Conversely, shRNA directed against Bnip3 or a mutant of Bnip3 defective for mitochondrial targeting abrogated DOX-induced loss of COX1-UCP3 complexes and respiratory chain defects. Finally, Bnip3$^{-/-}$ mice treated with DOX displayed relatively normal mitochondrial morphology, respiration, and mortality rates comparable to those of saline-treated WT mice, supporting the idea that Bnip3 underlies the cardiotoxic effects of DOX. These findings reveal a new signaling pathway in which DOX-induced mitochondrial respiratory chain defects and necrotic cell death are mutually dependent on and obligatorily linked to Bnip3 gene activation. Interventions that antagonize Bnip3 may prove beneficial in preventing mitochondrial injury and heart failure in cancer patients undergoing chemotherapy.

ventricular myocytes | mitochondria | cell death | heart failure | Bnip3

Doxorubicin (DOX) and related anthracyclines are widely used in chemotherapeutic regimens to treat childhood and adult malignancies (1, 2). Despite the clinical efficacy of these agents, however, it is well established that cancer patients undergoing DOX treatment are susceptible to acute and chronic cardiac anomalies, including aberrant arrhythmias, ventricular dysfunction, and heart failure (1, 2). Thus, a major challenge in managing cancer patients treated with DOX is to minimize DOX's cardiotoxic effects without compromising its antitumor properties. The molecular signaling pathways that underlie the cardiotoxic effects of DOX remain cryptic. Several theories, including mitochondrial dysfunction, increased reactive oxygen species (ROS) production, defects in iron handling, and contractile failure, have been proposed as plausible underlying mechanisms (3–5). Moreover, certain transcription factors involved in the regulation of genes crucial for vital processes, including metabolism and cell survival, are known to be altered during DOX treatment (6, 7).

Despite these findings, however, a unifying explanation for the cardiotoxic effects of DOX has not been advanced. Thus, information regarding the signaling pathways and molecular effectors that underlie the cardiotoxic effects of DOX is limited. In this regard, mitochondrial injury induced by DOX has been reported (5). The mitochondrion plays a central role in regulating energy metabolism and cellular respiration, and was recently identified as a signaling platform for cell death by apoptosis and necrosis, respectively (8). Given that the mitochondrion regulates these vital cellular processes, we reasoned that it may be a convergence point for the cytotoxic effects of DOX. This view is supported by a recent report demonstrating impaired mitochondrial iron transport and ROS production by DOX (3). The signaling pathways and molecular effectors that impinge on the mitochondrial defects associated with DOX toxicity remain undetermined.

Previous work by our laboratory established the Bcl-2-like 19kDa-interacting protein 3 (Bnip3) as a critical regulator of mitochondrial function and cell death of cardiac myocytes during hypoxic injury (9). Indeed, Bnip3 gene activation can trigger mitochondrial perturbations consistent with mitochondrial permeability transition pore (mPTP) opening, loss of mitochondrial membrane potential ($\Delta\Psi m$), and cell death with features of necrosis (9, 10). Notably, genetic interventions that antagonize the expression or integration of Bnip3 into mitochondrial

Significance

We provide new, exciting evidence for a previously unidentified signaling pathway that mechanistically links mitochondrial respiratory chain defects to necrosis and heart failure induced by the chemotherapy agent doxorubicin (DOX). We specifically show that DOX disrupts protein complexes between the key respiratory chain proteins, including uncoupling protein 3 and cytochrome *c* oxidase, resulting in abnormal mitochondrial respiration and necrosis through a mechanism contingent on Bcl-2-like 19kDa-interacting protein 3 (Bnip3). Perhaps most compelling is our finding that inhibiting Bnip3 completely abrogated the cardiotoxic effects of DOX. These exciting findings have important clinical implications not only for preventing heart failure by targeting Bnip3 in cancer patients undergoing chemotherapy, but also for understanding the pathogenesis of other diseases in which mitochondrial function is compromised.

Author contributions: R.D. and L.A.K. designed research; R.D., V.M., S.R.C., and J.T. performed research; R.D., S.R.C., P.F., and G.W.D. contributed new reagents/analytic tools; R.D., V.M., S.R.C., J.T., and D.J. analyzed data; and R.D. and L.A.K. wrote the paper.

The authors declare no conflict of interest.

*This Direct Submission article had a prearranged editor.

[1]To whom correspondence should be addressed. Email: lorrie@sbrc.ca.

This article contains supporting information online at www.pnas.org/lookup/suppl/doi:10.1073/pnas.1414665111/-/DCSupplemental.

membranes are each sufficient to suppress mitochondrial defects and cell death of ventricular myocytes in vitro and in vivo (11). Moreover, Bnip3 can promote autophagy/mitophagy in certain cells; however, this property of Bnip3 is obscure and likely occurs in a cell- and context-specific manner, given that we and others have found that Bnip3 can promote maladaptive autophagy, resulting in cell death (10, 12, 13).

In contrast to other Bcl-2 death proteins that are constitutively expressed under basal conditions but require posttranslational signals for activation, the Bnip3 promoter is strongly repressed under basal conditions, owing to the presence of inhibitory repressor complexes that block Bnip3 transcription (14). Considering that the Bnip3 promoter is activated during metabolic stress, we reasoned that Bnip3 may underlie the mitochondrial injury and cardiotoxic effects associated with DOX. In the present work, we tested this possibility and found new, compelling evidence that Bnip3 is a molecular effector of DOX-induced cardiotoxicity in vivo and in vitro. We show that mechanistically, DOX triggers the loss of mitochondrial uncoupling protein 3 (UCP3) and cytochrome *c* oxidase (COX) subunit 1 (COX1) complexes, impairs respiratory capacity, and promotes necrotic cell death of ventricular myocytes through a mechanism that is mutually dependent on and obligatorily linked to Bnip3.

Materials and Methods

Cell Culture and Transfection. Postnatal rat cardiac myocytes were isolated from 1- to 2-d-old Sprague–Dawley rats and subjected to primary culture as described previously. Cells were treated with DOX (5 or 10 μM; Pfizer) for 18 h. Cells were infected with adenoviruses encoding Bnip3 shRNA or a carboxyl terminal domain mutant of Bnip3 defective for mitochondrial targeting, designated Bnip3ΔTM, as reported previously (10, 15, 16).

DOX Treatment in Vivo. Mice germ lines deleted for Bnip3 were characterized and reported previously (11). WT or Bnip3$^{-/-}$ mice aged 8–10 wk received a single i.p. injection of 0.9% physiological saline (vehicle control) or DOX (20 mg/kg) as described previously (17). Serial echocardiography was performed on all mice at baseline and daily for up to 10 d after saline or DOX treatment. Cardiac chamber size, left ventricular function, and endocardial peak velocity (V_{endo}) were evaluated by tissue Doppler imaging (18). Mice exhibiting a V_{endo} <1 cm/s were killed as a humane endpoint (18, 19). Hearts from saline-treated and DOX-treated mice were excised and processed for ultrastructural analysis by electron microscopy as reported previously (20, 21). In brief, hearts were fixed in 2% (wt/vol) glutaraldehyde and cut into <1-mm cubes from four random areas of the left ventricle free wall between the midregion and apex. Tissues were osmicated in 2% OsO_4, followed by standard tissue embedding in Epon. Ultrathin sections from WT and Bnip3 $^{-/-}$ mice were stained with uranyl acetate and lead citrate and examined for ultrastructural details. A total of 3,000 cells for each condition were analyzed. Cardiac cell lysate and RNA from hearts were processed for Western blot and quantitative PCR (qPCR) analyses, as reported previously (10).

Cell Viability. Postnatal ventricular cardiomyocytes were stained with the vital dyes calcein acetoxymethylester (calcein-AM) and ethidium homodimer-1 (each 2 μM) to visualize live (green) and dead (red) cells, respectively, by epifluorescence microscopy. At least ≥200 cells were counted from three independent experiments using three replicates for each condition tested. Data are expressed as the mean ± SE percent of dead cells from control (22). Lactate dehydrogenase (LDH) (Sigma-Aldrich) was assessed in the supernatant collected from the saline- or DOX-treated cells and from mouse serum, in accordance with the manufacturer's instructions. cardiac troponin T (cTnT) was assessed by immunoassay (Troponin T kit 04491815 and Cobas e 601 analyzer; Roche Diagnostics). High-mobility group box 1 (HMGB1) protein was detected by immunostaining of cardiac myocytes using a rabbit antibody directed against HMGB1 (1:50 dilution; Cell Signaling) and secondary goat anti-rabbit conjugated Alexa Fluor 488 (1:1,000; Molecular Probes).

Western Blot Analysis and Immunoprecipitation. Western blot analysis was performed for protein expression on cell lysate extracted from cardiac myocytes as reported previously. Protein extracts were resolved on denaturing SDS/PAGE gels transferred to nitrocellulose membranes. The filters were probed with primary murine antibody directed against Bnip3 as reported previously. All antibodies were used at 1:1,000 dilution in 2% BSA containing 0.1% TBS-T overnight at 4 °C. Bound proteins were detected using secondary HRP-conjugated anti-mouse or anti-rabbit antibodies by enhanced ECL (Pharmacia) (23). For immunoprecipitation studies, ventricular myocyte lysate was immunoprecipitated using SantaCruz Immunoprecipitation kit and antibodies to UCP3 (Sigma-Aldrich; catalog no. U7757) or COX1 (Abcam; catalog no. ab14705).

mPTP Opening, Mitochondrial ΔΨM, ROS, and Mitochondrial Calcium. To monitor mPTP opening, myocytes were incubated with 5 μmol/L calcein-AM (Molecular Probes) in the presence of 2–5 mmol/L cobalt chloride, as reported previously (24). Changes in integrated fluorescence intensity served as an index of mPTP opening. Cells were visualized with an Olympus AX-70 Research fluorescence microscope. Mitochondrial ΔΨM was assessed by epifluorescence microscopy by incubating cells with 50 nM tetra-methyl-rhodamine methyl ester perchlorate (TMRM) (Molecular Probes) (22). To monitor ROS production, cells were incubated with 2.5 μM dihydroethidium (Molecular Probes). Cells were visualized by epifluorescence microscopy as described previously (24). Mitochondrial calcium loading in cardiac myocytes in the absence and presence of DOX was assessed by monitoring dihydro-rhodamine-2 fluorescence (Molecular Probes), as reported previously (25).

Mitochondrial Respiration in Vitro and in Vivo. Mitochondrial OCR was assessed with a Seahorse XF24 Analyzer. In brief, cardiomyocytes were cultured in 24-well plates, followed by the sequential addition of oligomycin (1 μM), FCCP (2-[2-[4-(trifluoromethoxy)phenyl]hydrazinylidene]-propanedinitrile) (1 μM), and rotenone (1 μM) combined with antimycin (1 μM) as reported previously (26). After OCR measurement, cells were fixed and stained with Hoechst 33258 nuclear dye. Plates were scanned to quantify cell numbers using a Cellomics ArrayScan VTI HCS Reader (Thermo Scientific). OCR was normalized to cell number per respective well. For in vivo mitochondrial respiration, mitochondria were isolated from mouse hearts as described previously (27) and analyzed for respiration with the Seahorse analyzer. Data are expressed as mean ± SEM %OCR from three to five replicates.

Statistical Analysis. Multiple comparisons between groups were tested using one-way ANOVA. Bonferroni post hoc tests were used to determine differences among groups. The unpaired two-tailed Student *t* test was used to compare mean differences between two groups. Differences were considered statistically significant to a level of $P < 0.05$. For all in vitro studies, data were obtained from at least three or four independent myocyte isolations; for in vivo studies, data were obtained from 10–15 mice per group for each condition tested unless indicated otherwise.

Results

Cardiac Ultrastructure and Mitochondrial Dysfunction in DOX-Treated Mice. As a step toward understanding the molecular mechanisms underlying the cardiotoxic effects of DOX, we assessed the impact of DOX treatment on cardiac structure and function in vivo. In contrast to vehicle-treated mice, DOX-treated mice exhibited impaired cardiac function and severe ultrastructural defects, including disrupted sarcomeres, swollen mitochondria with loss of cristae, and extensive vacuolization (Fig. 1*A*). Notably, in the DOX-treated mice, heart mitochondria were severely impaired with respect to respiratory function, as evidenced by a marked reduction in mitochondrial basal respiration rates compared with mitochondria derived from vehicle-treated mice (Fig. 1*B*). Furthermore, a significant increase in serum LDH release, indicative of necrotic cell injury, was observed in the DOX-treated mice (Fig. 1*C*).

DOX Triggers Mitochondrial Perturbations and Necrotic Cardiac Cell Death. Based on the extensive mitochondrial and cell injury induced by DOX in vivo, we tested the impact of DOX on mitochondrial function and cell viability in postnatal ventricular mycoytes in vitro. Mitochondrial perturbations consistent with mPTP opening and loss of ΔΨm were observed in DOX-treated cardiac myocytes (Fig. 2*A*). Furthermore, vital staining of cells revealed a marked dose-dependent decline in cell viability in DOX-treated cells compared with vehicle-treated control cells (Fig. 2 *B* and *C*), a finding consistent with the DOX-induced mitochondrial defects. In addition, necrosis markers, including loss of nuclear HMGB1 (Fig. 2*D*), and release of LDH and cTnT were observed in cardiac myocytes treated with DOX. These

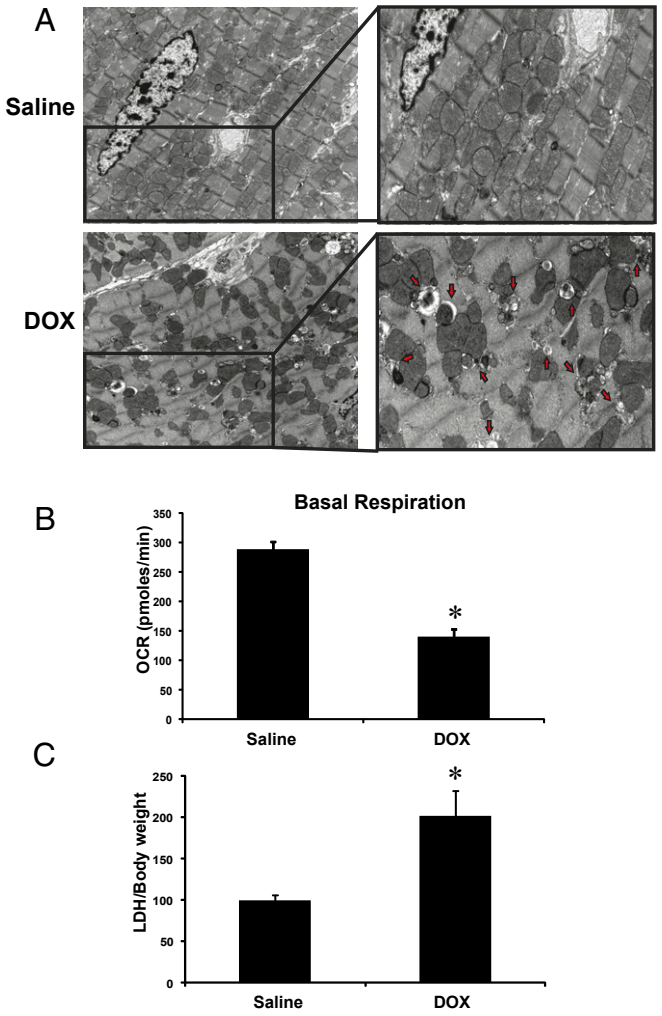

Fig. 1. DOX provokes ultrastructural defects and mitochondrial injury in vivo. (*A*) Representative electron micrograph images of murine cardiac muscle derived from mice treated with saline or DOX (single i.p injection, 20 mg/kg) at day 5 postinjection. (*Upper Left*) Saline-treated control mice. (*Upper Right*) Magnified section showing normal cardiac ultrastructure. (*Lower Left*) Representative mouse hearts after DOX treatment. (*Lower Right*) Magnified section showing ultrastructural defects including disrupted sarcomeres, mitochondrial swelling, and vacuolization. Red arrows denote membrane structures indicative of autophagosomes. (Magnification: 5,800×.) (*B*) Basal respiration of cardiac mitochondria derived from vehicle- and DOX-treated mouse hearts. OCR was measured with a Seahorse metabolic analyzer (*Materials and Methods*). (*C*) Serum LDH release from mice treated with saline or DOX. Data are presented as mean ± SEM. $P < 0.05$. *Statistically different from saline treatment.

findings are in agreement with our in vivo data and suggest that DOX triggers mitochondrial perturbations and necrotic death of cardiac myocytes.

Bnip3 Is Activated in Ventricular Myocytes Treated with DOX. We previously established that the inducible death protein Bnip3 provoked mitochondrial perturbations and cell death of cardiac myocytes with features of necrosis (10, 28). Because the mitochondrial injury induced by DOX is consistent with mitochondrial defects induced by Bnip3, we reasoned that DOX-induced mitochondrial injury may involve Bnip3. To formally test this possibility, we first assessed whether Bnip3 mRNA and protein expression levels were altered in postnatal ventricular myocytes in vivo and in vitro after DOX treatment. As demonstrated by qPCR and Western blot analysis (Fig. 3 *A* and *B*), compared with vehicle-treated mice, DOX-treated mice exhibited markedly increased Bnip3 mRNA and protein expression levels. Furthermore, a dose-dependent increase in Bnip3 protein expression was observed in ventricular myocytes treated with DOX in vitro (Fig. 3*C*), a finding consistent with our in vivo data.

Earlier work by our laboratory established the localization of Bnip3 to mitochondria via its carboxyl-terminal transmembrane domain as a crucial factor provoking mitochondrial defects and cell death of ventricular myocytes (29). Thus, we tested whether the association of Bnip3 and mitochondria is altered in cells treated with DOX. Bnip3 was detected in the S-100 cytoplasmic and mitochondrial fraction of vehicle-treated control cells (Fig. 3*D*), but was preferentially detected in the mitochondrial fraction of cells treated with DOX, a finding concordant with our previously published work on the increased mitochondrial localization of Bnip3 under stress conditions (9).

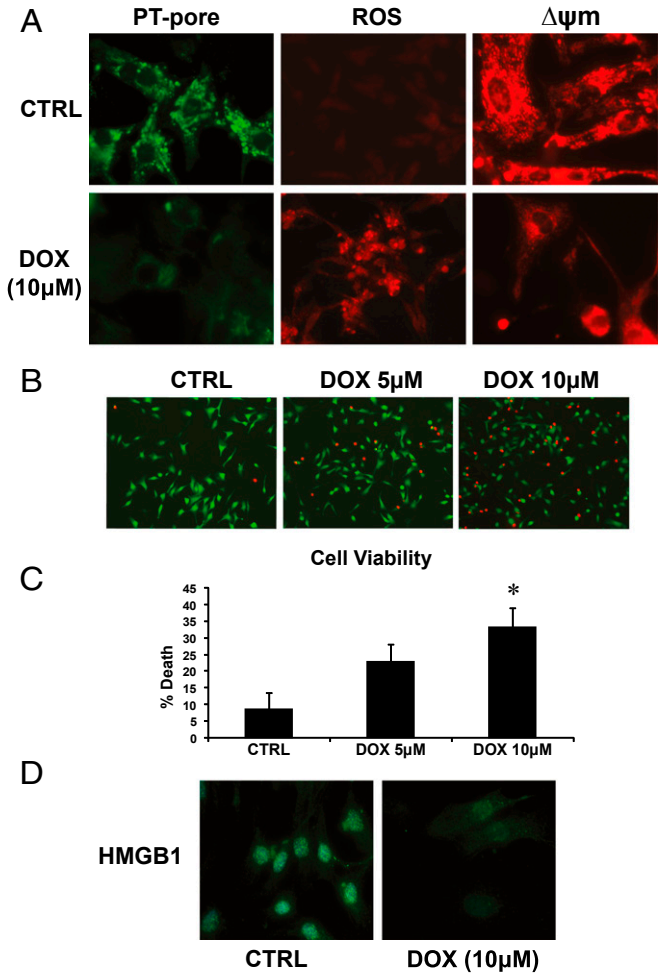

Fig. 2. DOX triggers mitochondrial perturbations and necrotic death of cardiac myoctyes. (*A*) Epifluorescence microscopy of control (CTRL) and DOX-treated cells for mPTP opening (*Left*), ROS (*Center*), and mitochondrial ΔΨm (*Right*); see *Materials and Methods* for details. (*B*) Cell viability of ventricular myocytes stained with vital dyes calcein-AM and ethidium-homodimer to detect the live (green) and dead (red) cells, respectively, in the absence and presence of DOX treatment (5 and 10 μM) for 18 h. (*C*) Histogram of the quantitative data in *B*. Data are expressed as mean ± SEM from at least four independent cell culture experiments counting ≥200 cells for each condition tested. $P < 0.05$. *Statistically different from control. (*D*) Epifluorescence microscopy of cardiac myocytes stained for nuclear HMGB1 protein (green nuclear staining) in vehicle-treated control cells and cells treated with DOX (10 μM) for 18 h.

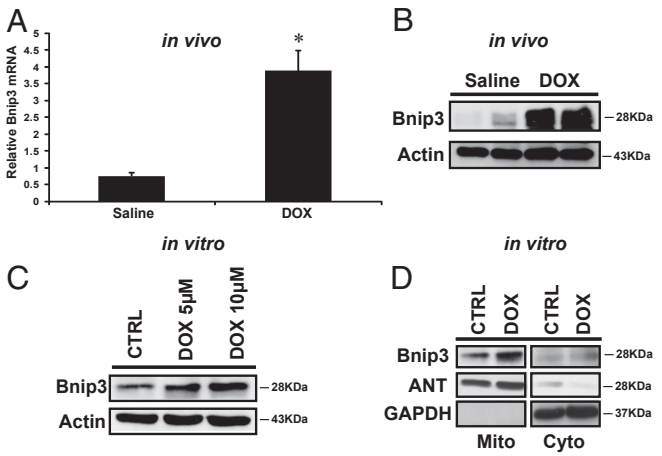

Fig. 3. DOX induces Bnip3 expression in ventricular myocytes. (*A*) Bnip3 mRNA expression in hearts from saline-treated control (CTRL) and DOX-treated mice; see *Materials and Methods* for details. $P < 0.05$. *Statistically different from saline control. (*B*) Western blot analysis of cardiac lysate for Bnip3 protein for conditions detailed in *A*. (*C*) Western blot analysis of cell lysate derived from isolated ventricular myocytes treated with DOX (5 and 10 μM) for 18 h or vehicle-treated control. The filter was probed with antibodies directed against Bnip3 and β-actin as a loading control for the Western blot analysis. (*D*) Western blot analysis of mitochondrial (Mito) and cytoplasmic s-100 (Cyto) fractions from cardiac myocytes in the absence and presence of DOX treatment. The filter was probed with antibody directed against Bnip3. Antibodies directed against mitochondrial protein adenine nucleotide transporter (ANT) and cytosolic protein GAPDH were used to verify the purity of cell fractionation.

DOX Disrupts Mitochondrial COX1-UCP3 Complexes and Respiration. The transfer of electrons via electron transport chain complexes on the inner mitochondrial membrane is essential for establishing the electromotive force and proton gradient for maintaining mitochondrial ΔΨm. Given that mitochondrial-associated Bnip3 disrupts ΔΨm, we reasoned that the observed loss of ΔΨm and increased ROS in cells treated with DOX might be related to a disruption of respiratory chain activity. To test this possibility, we assessed mitochondrial respiration in control cells and DOX-treated cells. Compared with vehicle-treated cells, the DOX-treated cells exhibited a marked reduction in maximal respiratory capacity, as evidenced by reduced oxygen consumption (Fig. 4 *A* and *B*). The DOX-treated cells had an almost negligible respiratory reserve capacity, indicating severely impaired mitochondrial respiration (Fig. 4*C*). Interestingly, mitochondrial respiration and reserve respiratory capacity (RRC) were similarly impaired in cells overexpressing Bnip3 (Fig. 4 *D–F*), a finding concordant with impaired mitochondrial respiration and loss of ΔΨm in the DOX-treated cells. Mitochondrial respiration involves electron transport chain complexes I–IV. Notably, COX or complex IV, the terminal complex required for reduction of molecular oxygen in normal cells, is composed of 13 individual subunits. The catalytic activity of COX1 is required for reduction of molecular oxygen to water. Preliminary studies revealed protein interactions between COX1 and UCP3.

Because uncoupling proteins are important regulators of ΔΨm and ROS, we tested whether the observed loss of ΔΨm and increased ROS in DOX-treated cells is related to alterations in COX1-UCP3 complexes. As shown on Western blot analysis (Fig. 4*E*), compared with vehicle-treated control cells, DOX-treated cells exhibited markedly reduced interactions between COX1 and UCP3, a finding consistent with our data showing increased ROS in DOX-treated cells (Fig. 2*A*). Taken together, these findings suggest that DOX disrupts COX1–UCP3 interactions and impairs respiration.

DOX Provokes Mitochondrial Perturbations Contingent on Bnip3. To explore the possibility that Bnip3 underlies the mitochondrial defects induced by DOX, we tested whether suppressing Bnip3 would influence the mitochondrial perturbations and cell death induced by DOX. For these studies, we used shRNA directed against Bnip3, which we had previously demonstrated to selectively and efficiently knockdown Bnip3 expression in cardiac myocytes (23, 24). shRNA directed against Bnip3 suppressed DOX-induced mitochondrial perturbations, including mPTP opening, ROS production, and loss of ΔΨm (Fig. 5 *A–D*). Further Western blot analyses (Fig. 5*E*) verified knockdown of Bnip3 in DOX-treated cells under the conditions shown in Fig. 5*A*.

Importantly, either knockdown of Bnip3 by shRNA or a carboxyl terminal transmembrane domain mutant of Bnip3 (Bnip3ΔTM), previously shown by our laboratory to be defective for integrating into mitochondria in cardiac myocytes and provoking cell death (9), normalized mitochondrial calcium (Fig. 6*A*). Perhaps most compelling is our finding that loss of COX1-UCP3 complexes in cells treated with DOX was completely restored by the Bnip3ΔTM mutant defective for mitochondrial integration

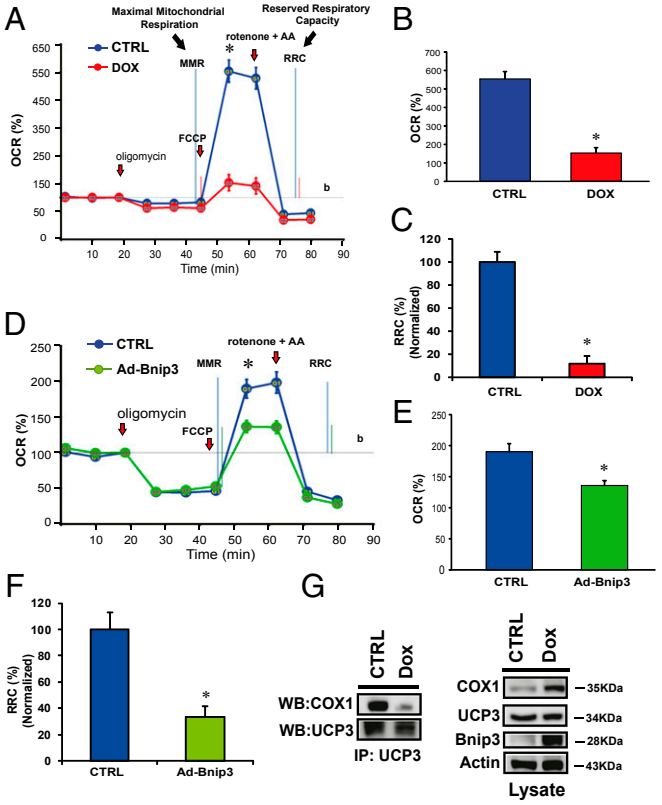

Fig. 4. DOX disrupts the interaction between mitochondrial COX1 and UCP3 and impairs respiration. (*A* and *B*) OCR was measured with a Seahorse metabolic analyzer. Oligomycin (1 μM), FCCP (1 μM), and rotenone (1 μM) combined with antimycin (1 μM) were added sequentially to saline-treated control (CTRL) (blue) or DOX-treated cardiomyocytes (red). b, baseline. (*B* and *C*) Histograms showing %OCR (*B*) and %RRC (*C*) data for *A*. Values are mean ± SEM from three to five replicates. $P < 0.05$. *Statistically different from control. (*D*) Respiration measurements in cardiomyocytes infected with adenoviral control vector (CTRL; blue) or adenovirus encoding Bnip3 cDNA (Ad Bnip3; green). (*E* and *F*) Histograms showing %OCR (*E*) and %RRC (*F*). $P < 0.05$. *Statistically different from control. (*G*) Effects of DOX on COX1 and UCP3 complex. (*Left*) Protein lysate derived from control and DOX-treated ventricular myocytes was immunoprecipitated with an antibody directed against UCP3 (1 μg/mL) and blotted with antibody directed against COX1. (*Right*) Western blot analysis of cell lysate used for immunoprecipitation and analyzed for expression of COX1, UCP3, Bnip3, and α-actin proteins.

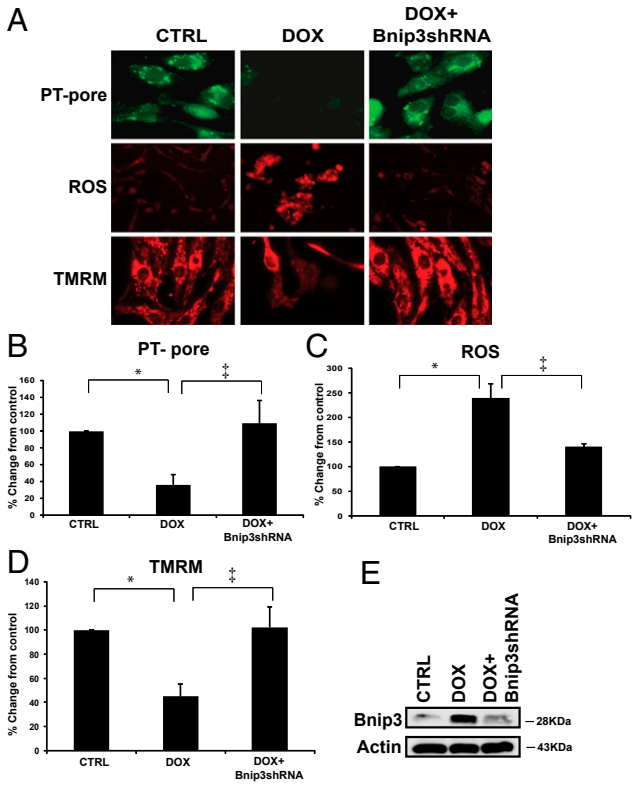

Fig. 5. DOX provokes mitochondrial perturbations contingent on Bnip3. Shown are mitochondrial perturbations induced by DOX in the absence or presence of Bnip3 knockdown. (*A, Top*) Epifluorescence microscopy of cardiac myocytes assessed for mPTP by mitochondrial calcein-AM-$CoCl_2$ (green). Loss of green fluorescence is indicative of mPTP opening. (*Middle*) Epifluorescence microscopy of ROS as assessed by dihydroethidine (red). (*Bottom*) Epifluorescence microscopy of cardiac myocytes assessed for mitochondrial $\Delta\Psi m$ by TMRM (red); see *Methods* for details. (*B–D*) Histograms for quantitative data for conditions shown in *A*. Data were obtained from three independent myocyte isolations using two replicates for each condition tested. $P < 0.05$. *Statistically different from control. ‡Statistically different from DOX-treated. (*E*) Western blot analysis of cardiac cell lysate derived from vehicle-treated control or DOX-treated cells in the absence and presence of shRNA directed against endogenous Bnip3 (14). The filter was probed with a murine antibody directed against Bnip3 to verify Bnip3 knockdown.

(Fig. 6*B*). In this context, the dimerization of Bnip3ΔTM with endogenous Bnip3 would sequester Bnip3 activity, thereby acting as a dominant-negative inhibitor of Bnip3 (9). Western blot analysis confirmed that WT Bnip3 was localized to the mitochondrial fraction, whereas the Bnip3ΔTM mutant was absent from mitochondria and detected mainly in the cytoplasmic fraction (Fig. 6*C*), a finding concordant with our previous work (9, 29). Furthermore, knockdown of Bnip3 restored maximal mitochondrial respiration (MMR) and RRC (Fig. 6 *D* and *E*), as well as cell viability, in DOX-treated cells (Fig. 7 *A* and *B*). Notably, DOX treatment induced a significant increase in necrosis markers, including release of LDH and cTnT, and knockdown of Bnip3 suppressed DOX-induced LDH and cTnT release (Fig. 7 *C* and *D*). Taken together, these findings strongly suggest that Bnip3 triggers mitochondrial injury and necrotic cell death induced by DOX.

DOX-Induced Necrotic Cell Injury Is Contingent on Bnip3 in Vivo. To verify the physiological significance of our in vitro findings, we tested the impact of DOX on WT mice and mice with a germ line deleted for Bnip3 in vivo. In contrast to WT mice treated with DOX, which exhibited severe ultrastructural defects, including misaligned sarcomeres, disrupted mitochondrial cristae, vacuolization, and increased serum LDH release, the $Bnip3^{-/-}$ mice were relatively resistant to DOX treatment, displaying normal cardiac ultrastructure, intact mitochondrial cristae, minimal vacuolization, and reduced serum LDH release (Fig. 8 *A* and *B*). Moreover, a marked increase in Bnip3 gene expression was observed in WT mice treated with DOX, a finding concordant with the serve ultrastructural defects in these hearts. Furthermore, Bnip3 mRNA was not detected in $Bnip3^{-/-}$ mice in absence or presence of DOX, verifying as a housekeeping control that the $Bnip3^{-/-}$ mice indeed were genetically null for Bnip3 (Fig. 8*C*). In addition, in contrast to vehicle-treated WT mice, DOX-treated mice exhibited mitochondrial respiratory chain defects, including reduced MMR and RRC, indicating severely impaired mitochondrial respiration is severely impaired (Fig. 9 *A–C*). Importantly, DOX-treated $Bnip3^{-/-}$ mice

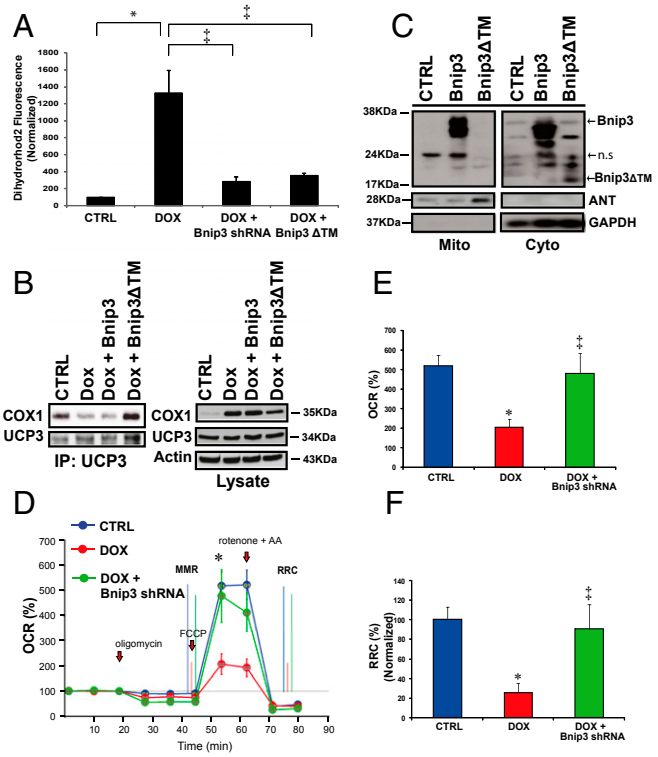

Fig. 6. Inhibition of Bnip3 rescues DOX-induced mitochondrial dysfunction. (*A*) Mitochondrial calcium content was assessed by epifluorescence microscopy using dihydrorhodamine 2 fluorescence for control (CTRL) or cells treated with DOX in the absence and presence of shRNA directed against Bnip3 or a carboxyl-terminal transmembrane mutant of Bnip3 defective for mitochondrial targeting (Bnip3ΔTM). The histogram shows relative integrated optical fluorescence. $P < 0.05$. *Statistically different from control. ‡Statistically different from DOX-treated. (*B, Left*) Immunoprecipitation of UCP3 was performed from the lysate derived from vector control cardiac myocytes and myocytes treated with DOX in the absence and presence of eukaryotic expression vectors for Bnip3 WT (Bnip3WT) or Bnip3ΔTM mutant. Cell lysate was immunoprecipitated with an antibody directed against UCP3 (Sigma-Aldrich). The filter was probed with antibody directed against COX1. (*Right*) Western blot analysis of cell lysate used for immunoprecipitation. The filter was probed for COX1, UCP3, and α-actin. (*C*) Western blot analysis of mitochondrial and cytoplasmic s-100 fractions of cells expressing Bnip3WT and Bnip3ΔTM mutant. Adenine nucleotide translocase (ANT) and GAPDH were used to verify the completeness of mitochondrial and cytoplasmic fractions, respectively. ns, nonspecific. (*D*) Mitochondrial respiration in vehicle control (CTRL, blue), DOX (red), and DOX + Bnip3shRNA (green). b, baseline. (*E* and *F*) Histograms showing %OCR (*E*) and %RRC (*F*) for the data in *D*. Values are mean ± SEM from two or three experiments using five replicates. $P < 0.05$. *Statistically different from control. ‡Statistically different from DOX-treated.

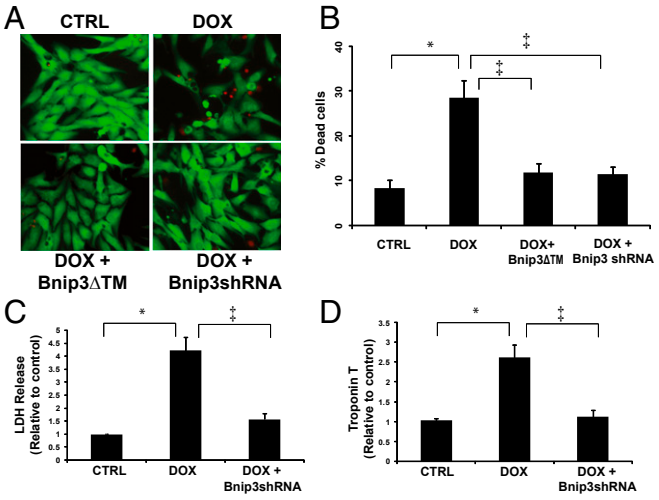

Fig. 7. Bnip3 gene silencing suppresses DOX-induced necrotic cell death. (*A*) Epifluorescence microscopy for cell viability, living cells (green), dead cells (red) for ventricular myocytes in the absence or presence of DOX (10 μM) with and without Bnip3 knockdown with shRNA directed against Bnip3 or Bnip3ΔTM mutant defective for mitochondrial targeting and vehicle-treated control cells (CTRL). (*B*) Histogram showing quantitative data for the conditions in *A*. Data were obtained from at least three independent myocyte isolations of ≥200 for each condition tested. $P < 0.05$. *Statistically different from control. ‡Statistically different from DOX-treated. (*C* and *D*) LDH and c-TnT release from supernatants was assessed in control and DOX-treated ventricular myocytes in the absence or presence of Bnip3shRNA. $P < 0.05$. *Statistically different from control. ‡Statistically different from DOX-treated.

had normal respiratory indices that were indistinguishable from those measured in vehicle-treated WT or Bnip3$^{-/-}$ control mitochondria. Furthermore, DOX-treated Bnip3$^{-/-}$ mice exhibited relatively normal cardiac function (Fig. 9*D*). Importantly, the DOX-treated WT mice had a significantly higher mortality rate than the DOX-treated Bnip3$^{-/-}$ mice, approaching 90% by day 10 (Fig. 9 *E* and *F*). These findings are concordant with our in vitro data and strongly support our contention that Bnip3 underlies the cardiotoxic effects of DOX.

Discussion

The molecular mechanisms that underlie the cardiotoxic effects of DOX remain cryptic. Although several paradigms, including increased ROS production, calcium and iron overload, and altered gene expression, have been advanced as putative underlying mechanisms, to date none has provided a unifying explanation to account for the cellular defects (1, 3, 30–32). In this report, we provide new, compelling evidence that DOX provokes mitochondrial perturbations and cell death of ventricular myocytes through a mechanism that involves Bnip3. Furethermore, we reveal a novel signaling pathway that operationally links mitochondrial respiratory defects and necrotic cell death to the cardiotoxic effects of DOX.

We previously identified Bnip3 as critical regulator of mitochondrial function and cell death of cardiac myocytes during hypoxic stress (9, 10, 14). We attributed this function to mPTP opening and loss of mitochondrial ΔΨm triggered by the mitochondrial targeting of Bnip3. The finding that Bnip3 gene and protein expression are markedly increased by DOX is compelling and identifies Bnip3 as putative downstream effector of DOX toxicity. Indeed, the link between Bnip3 and the cytotoxic effects of DOX is profound, as demonstrated by the fact that WT mice treated with DOX exhibited severe ultrastructural defects, including disrupted sarcomeres, swollen mitochondria with loss of cristae, impaired mitochondrial respiration, and severe vacuolization consistent with autophagosomes, whereas DOX-treated Bnip3$^{-/-}$ mice were comparably resistant to the cytotoxic effects of DOX, exhibiting normal cardiac ultrastructure and mitochondria with intact cristae and normal respiration.

Based on the foregoing findings, our data support a model in which the cytotoxic effects of DOX are mediated by a mechanism involving Bnip3. Indeed, we have showed through not one, but three independent approaches that disruption of Bnip3 abrogates the mitochondrial perturbations and cell death of ventricular myocytes induced by DOX. This idea is concordant with the favorable cardiac function data and reduced mortality of DOX-treated Bnip3$^{-/-}$ mice.

We previously established that the mitochondrial targeting of Bnip3 is crucial for provoking mPTP opening and necrotic cell death of ventricular myocytes; however, the underlying mechanisms remained unclear (9, 10). Thus, another interesting and important aspect of the present study is our finding of dramatically increased mitochondrial-associated Bnip3 in cells treated with DOX, in concert with a marked reduction in COX1–UCP3 interaction, as well as loss of ΔΨm and increased ROS production. Uncoupling proteins play a critical role in the maintenance of mitochondrial ΔΨm, and UCP3 is the dominant uncoupling protein isoform in the heart (33). In contrast to UCP1, which

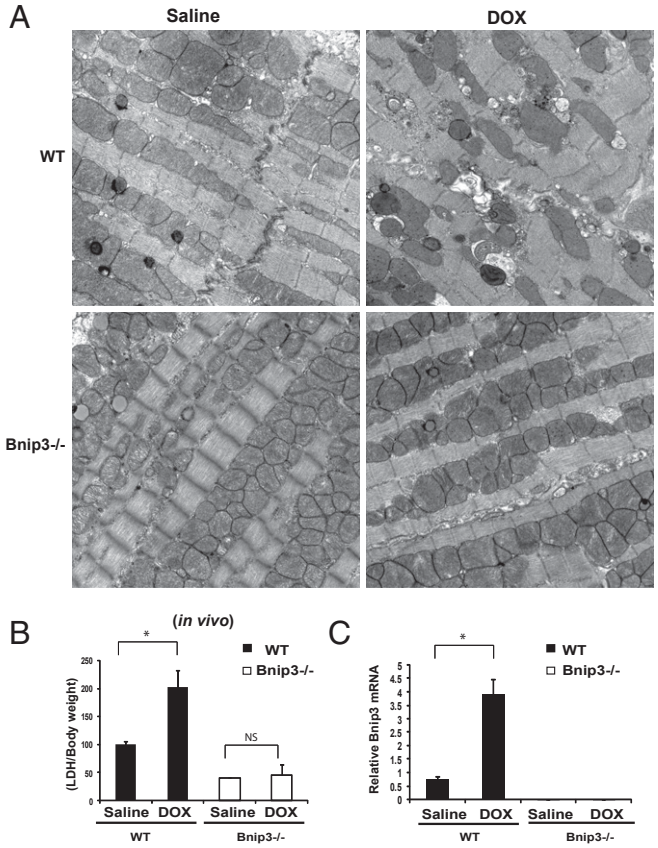

Fig. 8. DOX provokes mitochondrial injury contingent on Bnip3. (*A*) Representative electron micrographs of cardiac tissue derived from WT and Bnip3$^{-/-}$ mice treated with saline or DOX. (*Upper*, *Left*) Saline-treated WT mice. (*Upper*, *Right*) DOX-treated WT mice. (*Lower*, *Left*) Saline-treated Bnip3$^{-/-}$ mice. (*Lower*, *Right*) DOX-treated Bnip3$^{-/-}$ mice. (Magnification: 10,500×.) (*B*) Serum LDH release, expressed as LDH/body weight, from WT and Bnip3$^{-/-}$ mice treated with saline or DOX. (*C*) qPCR analysis of Bnip3 mRNA in WT mice and Bnip3$^{-/-}$ mice treated with saline or DOX. Data are expressed as mean ± SEM, fold change from saline-treated control. $P < 0.05$. *Statistically different from saline. ns, statistically nonsignificant.

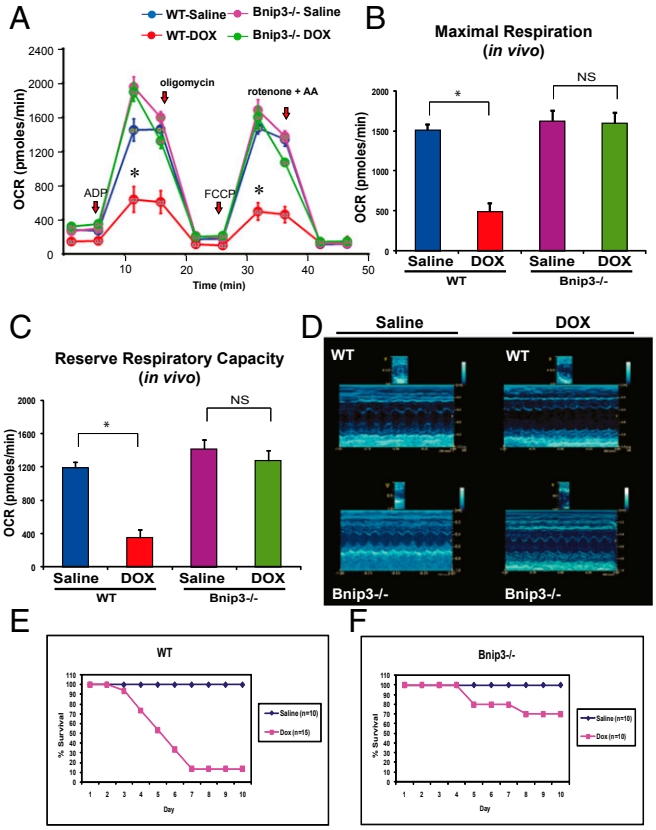

Fig. 9. Bnip3$^{-/-}$ mice are resistant to DOX-induced mitochondrial respiratory chain defects and cardiac dysfunction. (*A*) Respiratory rates of heart mitochondria isolated from surviving WT mice and Bnip3 $^{-/-}$ mice treated with vehicle or DOX after 10 d of treatment. OCR was measured with a Seahorse metabolic analyzer; details are provided in Fig. 4. Saline-treated WT mice are shown in blue; DOX-treated WT mice, in red; saline-treated Bnip3$^{-/-}$ mice, in pink; DOX-treated Bnip3$^{-/-}$ mice, in green. (*B* and *C*) Histograms showing relative MMR and RRC from data shown in *A*. Data are expressed as mean ± SEM. OCR (pmol/min) from 20 μg of isolated heart mitochondria from each condition tested, $n = 5$ replicates; $P < 0.05$. *Statistically different from vehicle-treated control. NS, statistically nonsignificant. (*D*, *Upper*) Representative M-mode echocardiography images of saline- and DOX-treated WT and Bnip3$^{-/-}$ mice at 5 d posttreatment. (*Lower*) M-mode images of Bnip3$^{-/-}$ mice from saline- and DOX-treated age-matched littermates. (*E* and *F*) Survival curves for vehicle- and DOX-treated WT (*E*) and Bnip3$^{-/-}$ (*F*) mice.

predominately regulates thermogenesis in brown adipose tissue, UCP2 and UCP3 regulate mitochondrial ΔΨm by balancing oxidative metabolism and respiration in skeletal and cardiac muscle by diverting proton flux across the mitochondrial inner membrane away from the F0/F1-ATPase (33, 34). Loss of UCP3 function promotes increased mitochondrial ROS production and loss of ΔΨm (33).

The finding that Bnip3 knockdown or a carboxyl transmembrane domain mutant of Bnip3 defective for integrating in mitochondrial membranes rescued disruption of COX1-UCP3 complexes, mitochondrial respiration, ROS production and other mitochondrial perturbations not only argues for the importance of COX1–UCP3 interaction in normal mitochondrial respiration, but also highlights its importance as critical downstream target of Bnip3 for DOX-induced mitochondrial dysfunction. In this regard, Morrill et al. (35) recently identified transmembrane helices within COX1, 2, and 3 critical for proton transport channels across the mitochondrial matrix and inner membrane space. Given that UCP3 also can influence proton flux across the inner mitochondrial membrane, the association of UCP3 and COX1 may play a critical role in regulating the proton gradient across the inner membrane space and matrix. This would invariably influence ROS production and ATP synthesis.

Consequently, based on the present study, we envision a model in which the integration of Bnip3 into mitochondrial membranes in DOX-treated cells would disrupt the integrity of the mitochondrial inner membrane, resulting in ROS production through loss of COX1-UCP3 complexes, mPTP opening, and necrotic cell death (Fig. S1). At present, however, whether the observed loss of COX1-UCP3 complexes and subsequent mitochondrial injury are regulated directly or indirectly by Bnip3 remains unclear. We did not assess protein–protein interactions in this study, but speculate that Bnip3 may displace COX1 from UCP3 or, alternatively, influence COX1–UCP3 associations by impinging other mitochondrial proteins, such as VDAC. This view is supported by a recent report demonstrating the ability of the carboxyl-terminal transmembrane domain of Bnip3 to engage the mitochondrial inner membrane (9, 36) and our present finding that a mutation of Bnip3 defective for mitochondrial targeting is sufficient to prevent disruption of the COX1-UCP3 complex in cells treated with DOX. The mechanism by which Bnip3 disrupts COX1–UCP3 association is unknown and is an active area of investigation in our laboratory. Nonetheless, our data strongly suggest that COX1-UCP3 complexes are disrupted in cells treated with DOX in manner contingent on Bnip3.

Another interesting finding of the present study is the presence of DOX-induced mitochondrial abnormalities consistent with mitophagy. Although autophagy/mitophagy was not the focus of this study, we observed a dramatic increase in vacuolization and double membrane structures containing mitochondria consistent with mitophagy in the hearts of mice after DOX treatment. The significance of this observation is unknown; however, autophagy beyond a certain threshold can promote death (16, 37–39). This is concordant with an earlier report demonstrating that DOX-induced autophagy is detrimental and promotes cell death (6). Concordant with this idea, autophagosomes were readily detected in hearts of DOX-treated WT mice, coinciding with necrosis; however, vacuolization and necrotic injury were virtually absent in the hearts of DOX-treated Bnip3$^{-/-}$ mice. These findings are in complete agreement with our cell viability data and the observed resistance of Bnip3$^{-/-}$ mice to DOX-induced injury. The fact that DOX induced autophagosomes in vivo as well as classical markers of necrosis (i.e., LDH and cTnT release) were normalized by inhibition of Bnip3 suggests that Bnip3 regulates both of these cellular processes. The finding that inner mitochondrial membrane integrity, which has been linked to mPTP opening and necrosis (40, 41), was abrogated by Bnip3 knockdown in cardiac myocytes treated with DOX strongly suggests that inner mitochondrial membrane defects induced by Bnip3 are likely the primary underlying defects associated with DOX cardiotoxicty. This idea is consistent with the fact that mitochondrial calcium loading, mPTP opening, and loss of mitochondrial ΔΨm in cells treated with DOX were normalized by inhibition of Bnip3. These findings support a model in which Bnip3 mediates the underlying cytotoxic effects of DOX by disrupting mitochondrial function (9, 10, 28). Based on our findings, it is tempting to speculate that because the heart is so abundantly rich in mitochondria, it is susceptible to DOX toxicity.

Our present findings demonstrate a novel signaling pathway that functionally links mitochondrial injury and cell death induced by DOX to Bnip3. Our data provide the first direct evidence that DOX induces cell death of cardiac myocytes through a mechanism that is obligatorily linked and mutually dependent on the mitochondrial injury induced by Bnip3. Thus, interventions designed to selectively inhibit Bnip3 signaling may prove beneficial in mitigating the cardiotoxic effects of DOX in cancer patients undergoing chemotherapy.

ACKNOWLEDGMENTS. We thank Dr. H. Weisman for critical comments on the manuscript and F. Aguilar, J. Gerstein, and J. Ryplanski for technical

assistance. This work was supported by NIH Grant HL 59888 (to G.W.D.) and grants to L.A.K. from the Canadian Institute for Health Research and the Heart and Stroke Foundation of Canada. L.A.K. is a Canada Research Chair in Molecular Cardiology.

1. Singal PK, Iliskovic N (1998) Doxorubicin-induced cardiomyopathy. *N Engl J Med* 339(13):900–905.
2. Singal PK, Li T, Kumar D, Danelisen I, Iliskovic N (2000) Adriamycin-induced heart failure: Mechanism and modulation. *Mol Cell Biochem* 207(1-2):77–86.
3. Ichikawa Y, et al. (2014) Cardiotoxicity of doxorubicin is mediated through mitochondrial iron accumulation. *J Clin Invest* 124(2):617–630.
4. Simůnek T, et al. (2009) Anthracycline-induced cardiotoxicity: Overview of studies examining the roles of oxidative stress and free cellular iron. *Pharmacol Rep* 61(1):154–171.
5. Berthiaume JM, Wallace KB (2007) Adriamycin-induced oxidative mitochondrial cardiotoxicity. *Cell Biol Toxicol* 23(1):15–25.
6. Kobayashi S, et al. (2010) Transcription factor GATA4 inhibits doxorubicin-induced autophagy and cardiomyocyte death. *J Biol Chem* 285(1):793–804.
7. Zhu W, Zhang W, Shou W, Field LJ (2014) P53 inhibition exacerbates late-stage anthracycline cardiotoxicity. *Cardiovasc Res* 103(1):81–89.
8. Mughal W, Dhingra R, Kirshenbaum LA (2012) Striking a balance: Autophagy, apoptosis, and necrosis in a normal and failing heart. *Curr Hypertens Rep* 14(6):540–547.
9. Regula KM, Ens K, Kirshenbaum LA (2002) Inducible expression of BNIP3 provokes mitochondrial defects and hypoxia-mediated cell death of ventricular myocytes. *Circ Res* 91(3):226–231.
10. Wang EY, et al. (2013) p53 mediates autophagy and cell death by a mechanism contingent on Bnip3. *Hypertension* 62(1):70–77.
11. Diwan A, et al. (2007) Inhibition of ischemic cardiomyocyte apoptosis through targeted ablation of Bnip3 restrains postinfarction remodeling in mice. *J Clin Invest* 117(10):2825–2833.
12. Gustafsson AB (2011) Bnip3 as a dual regulator of mitochondrial turnover and cell death in the myocardium. *Pediatr Cardiol* 32(3):267–274.
13. Hamacher-Brady A, Brady NR, Gottlieb RA, Gustafsson AB (2006) Autophagy as a protective response to Bnip3-mediated apoptotic signaling in the heart. *Autophagy* 2(4):307–309.
14. Shaw J, et al. (2006) Transcriptional silencing of the death gene *BNIP3* by cooperative action of NF-kappaB and histone deacetylase 1 in ventricular myocytes. *Circ Res* 99(12):1347–1354.
15. Yurkova N, et al. (2008) The cell cycle factor E2F-1 activates Bnip3 and the intrinsic death pathway in ventricular myocytes. *Circ Res* 102(4):472–479.
16. Maejima Y, et al. (2013) Mst1 inhibits autophagy by promoting the interaction between Beclin1 and Bcl-2. *Nat Med* 19(11):1478–1488.
17. Walker JR, et al. (2011) The cardioprotective role of probucol against anthracycline and trastuzumab-mediated cardiotoxicity. *J Am Soc Echocardiogr* 24(6):699–705.
18. Jassal DS, et al. (2009) Utility of tissue Doppler and strain rate imaging in the early detection of trastuzumab- and anthracycline-mediated cardiomyopathy. *J Am Soc Echocardiogr* 22(4):418–424.
19. Saeed MF, Premecz S, Goyal V, Singal PK, Jassal DS (2014) Catching broken hearts: Preclinical detection of doxorubicin- and trastuzumab-mediated cardiac dysfunction in the breast cancer setting. *Can J Physiol Pharmacol* 92(7):546–550.
20. Kirshenbaum LA, Singal PK (1992) Antioxidant changes in heart hypertrophy: Significance during hypoxia-reoxygenation injury. *Can J Physiol Pharmacol* 70(10):1330–1335.
21. Kirshenbaum LA, Singal PK (1992) Changes in antioxidant enzymes in isolated cardiac myocytes subjected to hypoxia-reoxygenation. *Lab Invest* 67(6):796–803.
22. Gurevich RM, Regula KM, Kirshenbaum LA (2001) Serpin protein CrmA suppresses hypoxia-mediated apoptosis of ventricular myocytes. *Circulation* 103(15):1984–1991.
23. Shaw J, et al. (2008) Antagonism of E2F-1 regulated Bnip3 transcription by NF-kappaB is essential for basal cell survival. *Proc Natl Acad Sci USA* 105(52):20734–20739.
24. Dhingra R, et al. (2013) Bidirectional regulation of nuclear factor-κB and mammalian target of rapamycin signaling functionally links Bnip3 gene repression and cell survival of ventricular myocytes. *Circ Heart Fail* 6(2):335–343.
25. Brandes R, Bers DM (2002) Simultaneous measurements of mitochondrial NADH and Ca(2+) during increased work in intact rat heart trabeculae. *Biophys J* 83(2):587–604.
26. Roy Chowdhury SK, et al. (2012) Impaired adenosine monophosphate-activated protein kinase signalling in dorsal root ganglia neurons is linked to mitochondrial dysfunction and peripheral neuropathy in diabetes. *Brain* 135(Pt 6):1751–1766.
27. Rogers GW, et al. (2011) High-throughput microplate respiratory measurements using minimal quantities of isolated mitochondria. *PLoS ONE* 6(7):e21746.
28. Vande Velde C, et al. (2000) BNIP3 and genetic control of necrosis-like cell death through the mitochondrial permeability transition pore. *Mol Cell Biol* 20(15):5454–5468.
29. Gang H, et al. (2011) A novel hypoxia-inducible spliced variant of mitochondrial death gene Bnip3 promotes survival of ventricular myocytes. *Circ Res* 108(9):1084–1092.
30. Iliskovic N, et al. (1999) Mechanisms of beneficial effects of probucol in adriamycin cardiomyopathy. *Mol Cell Biochem* 196(1-2):43–49.
31. Ky B, Vejpongsa P, Yeh ET, Force T, Moslehi JJ (2013) Emerging paradigms in cardiomyopathies associated with cancer therapies. *Circ Res* 113(6):754–764.
32. Rasbridge SA, et al. (1994) The effects of chemotherapy on morphology, cellular proliferation, apoptosis and oncoprotein expression in primary breast carcinoma. *Br J Cancer* 70(2):335–341.
33. Bézaire V, Seifert EL, Harper ME (2007) Uncoupling protein-3: Clues in an ongoing mitochondrial mystery. *FASEB J* 21(2):312–324.
34. Mailloux RJ, Harper ME (2012) Mitochondrial proticity and ROS signaling: Lessons from the uncoupling proteins. *Trends Endocrinol Metab* 23(9):451–458.
35. Morrill GA, Kostellow AB, Gupta RK (2014) The pore-lining regions in cytochrome *c* oxidases: A computational analysis of caveolin, cholesterol and transmembrane helix contributions to proton movement. *Biochim Biophys Acta* 1838(11):2838–2851.
36. Landes T, et al. (2010) The BH3-only Bnip3 binds to the dynamin Opa1 to promote mitochondrial fragmentation and apoptosis by distinct mechanisms. *EMBO Rep* 11(6):459–465.
37. Sciarretta S, Hariharan N, Monden Y, Zablocki D, Sadoshima J (2011) Is autophagy in response to ischemia and reperfusion protective or detrimental for the heart? *Pediatr Cardiol* 32(3):275–281.
38. Dhingra R, Kirshenbaum LA (2013) Mst-1 switches between cardiac cell life and death. *Nat Med* 19(11):1367–1368.
39. Rothermel BA, Hill JA (2008) Autophagy in load-induced heart disease. *Circ Res* 103(12):1363–1369.
40. Bernardi P, von Stockum S (2012) The permeability transition pore as a Ca(2+) release channel: New answers to an old question. *Cell Calcium* 52(1):22–27.
41. Whelan RS, et al. (2012) Bax regulates primary necrosis through mitochondrial dynamics. *Proc Natl Acad Sci USA* 109(17):6566–6571.